

A DUAL-BAND RF ENERGY HARVESTING USING FREQUENCY LIMITED DUAL-BAND IMPEDANCE MATCHING

Phirun Kim, Girdhari Chaudhary, and Yongchae Jeong*

Division of Electronics and Information Engineering, IT Convergence Research Center, Chonbuk National University, 567, Baekje-daero, Deokjin-gu, Jeonju-si, Jeollabuk-do, Chonbuk, 561-756, Republic of Korea

Abstract—In this paper, a novel dual-band RF-harvesting RF-DC converter with a frequency limited impedance matching network (M/N) is proposed. The proposed RF-DC converter consists of a dual-band impedance matching network, a rectifier circuit with villard structure, a wideband harmonic suppression low-pass filter (LPF), and a termination load. The proposed dual-band M/N can match two receiving band signals and suppress the out-of-band signals effectively, so the back-scattered nonlinear frequency components from the nonlinear rectifying diodes to the antenna can be blocked. The fabricated circuit provides the maximum RF-DC conversion efficiency of 73.76% and output voltage 7.09 V at 881 MHz and 69.05% with 6.86 V at 2.4 GHz with an individual input signal power of 22 dBm. Moreover, the conversion efficiency of 77.13% and output voltage of 7.25 V are obtained when two RF waves with input dual-band signal power of 22 dBm are fed simultaneously.

1. INTRODUCTION

Since the first wireless energy transmission was demonstrated experimentally in the 1890's by Nikola Tesla for lighting applications, the most part of the wireless transmission has been occupied for communication systems in the 20th century [1]. In recent years, the demands for wireless power transmission or RF energy harvesting have been growing for many applications. Moreover, a rectenna is one important component in wireless power transmission and has been used to provide DC power in wireless sensors [2–4].

Received 17 June 2013, Accepted 20 July 2013, Scheduled 28 July 2013

* Corresponding author: Yongchae Jeong (ycjeong@jbnu.ac.kr).

To achieve high conversion efficiency, the usage of multiple frequency bands, antenna arrays, dual-circularly polarized patch antenna, etc. have been developed [5–15]. In [5], circular sector rectenna which could suppress harmonics and eliminate the input LPF was reported. Power combining methods of the arrayed microwave rectifiers and compromise between a high conversion efficiency and weak RF power operation were discussed in [6–8]. In the rectifiers, the nonlinear rectifying elements also generate several harmonic current components in addition to DC, which can affect the RF-DC conversion efficiency [9–11]. Thus, the open or short harmonic terminations which can suppress the unwanted RF signals of Schottky diodes to obtain high efficiency were declared in [9].

In modern communication system, the usage of multiple frequency bands in wireless communication systems are growing, and some effort for dual-frequency rectennas has been made [11–17]. In [11, 17], to increase the energy harvesting efficiency, rectenna is required to match the impedance at both bands. Moreover, the dual-band rectenna was reported in this work by using separate rectifiers and impedance M/Ns, which is an advantage of the application demonstrated in [13]. However, two separate circuits would increase the overall circuit size and cost of the system. On the other hand, a dual-band printed dipole rectenna was developed for the wireless power transmission at 2.45 GHz and 5.8 GHz [14]. In this work, separate M/N and bandstop filters were used to block the reradiated harmonics generated by diodes at each band, which increased the cost and size of the system. In most of the previous works, the efficiency of RF-DC converters was enhanced by suppressing the harmonics with the LPF, bandpass filter, harmonic terminations, etc. However, none of the above referenced works focused on the design of an RF harvesting system using the dual-band impedance M/N that matched two operating bands simultaneously and suppressed the out-of-band signals.

In this paper, a novel design of dual-band RF-DC converter using a frequency limited dual-band impedance M/N is presented. The benefits of the proposed circuit are that the impedances at two different receiving frequencies can be matched, and the out-of-band nonlinear components can be blocked. To suppress the output harmonics generated by the nonlinear rectifier at the load, a wideband LPF is used. This paper is organized as follows. Section 2 describes the detail analysis of the frequency selective dual-band M/N, LPF, and RF-DC conversion circuit. Section 3 provides the measurement performance of the proposed dual-band RF harvesting system followed by a conclusion in Section 4.

2. ANALYSIS OF DUAL-BAND RF-DC CONVERSION SYSTEM

The proposed a high efficient dual-band RF-DC conversion circuit consisting of a dual-band impedance M/N, a rectifier circuit with a Villard structure, a harmonic suppression LPF, an output load network, and storage battery is shown in Fig. 1. The dual-band impedance M/N matches the antenna to the rectifier. The LPF suppresses the harmonics generated by the nonlinear diode characteristics.

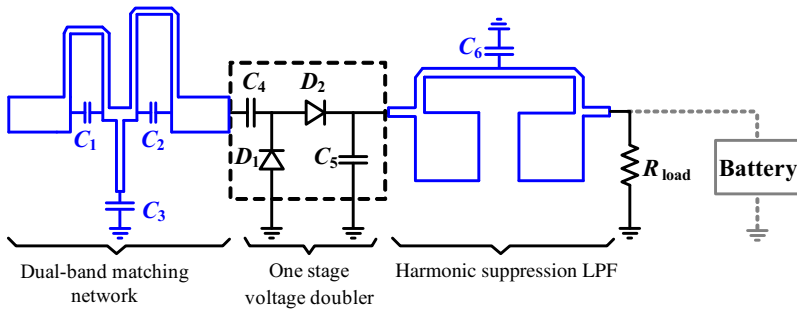


Figure 1. Configuration of high efficient dual-band RF-DC converter.

The RF-DC conversion efficiency is usually defined as the ratio of the total DC power delivered to the load to the receiving RF power [5–10, 14–17] as follows.

$$\eta = \frac{P_{DC}}{P_{RF}} = \frac{V_{DC}^2/R_{load}}{P_{RF}}, \quad (1)$$

where R_{load} , V_{DC} , and P_{RF} are the load resistance, output voltage, and incident RF power, respectively.

2.1. RF-DC Conversion Rectifier-circuit

Since the proposed circuit is designed for the microwave frequency as shown in Fig. 1, a fast switching time diode is required [9]. The Schottky diode uses a metal-semiconductor junction instead of a semiconductor-semiconductor junction, which allows to operate much fast and gives a forward voltage drop as low as 0.15 V. A saturated current is also a critical parameter since it is related to the RF-DC conversion efficiency of the diode rectifier. Therefore, it is desirable to have diodes with high-saturation current, low-junction capacitance, and low-series resistance for the RF-DC converter. Furthermore, the

diodes with higher saturation voltage also render a higher forward current, which is useful for the driving load.

The operation of the one stage Villard structure shown in Fig. 1 can be explained as follows. On the negative half-cycle of the input signal voltage, a capacitor C_4 is charged through the diode D_1 to a peak signal voltage. On the positive half-cycle, the capacitor C_5 is charged through the diode D_2 at about twice the peak of the signal voltage. Therefore, the output DC voltage of the general voltage doubling circuit is directly proportional to the number of stages given by [18, 19].

$$V_{OUT} = 2N(V_{IN} - \Delta V), \quad (2)$$

where V_{IN} , N , and ΔV are the peak voltage of the input signal, number of diode stages of the rectifier, and voltage drop across the diode, respectively. For the high efficient RF-DC converter, it is necessary to trade-off among these values. The measurements have been performed with one stage Villard structure without input M/N and LPF. The Schottky diode HSMS-2822 of the Avago, ceramic chip capacitors, and chip resistor are used in this measurement. Fig. 2(a) shows the output voltage and conversion efficiency of the RF-DC converter according to the R_{load} with the fixed capacitances (C_4 , C_5) and input power (P_{in}) 22 dBm. As seen in Fig. 2(a), the conversion efficiency is high in the range of R_{load} 0.33–0.433 k Ω and is decreased after 0.47 k Ω . However, the output voltage is linearly increased according to R_{load} . Therefore, a trade-off between high output voltage and high efficiency is required. The $R_{load} = 0.433$ k Ω has been chosen in this measurement. Fig. 2(b) shows the variation of the output voltage and efficiency according to

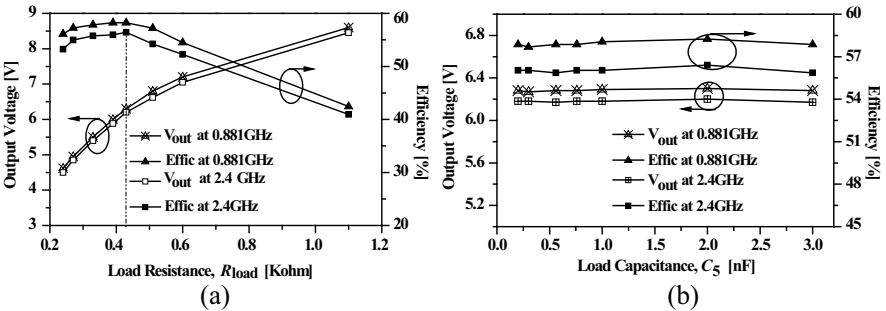


Figure 2. Measured RF-DC conversion efficiency and output voltage at $P_{in} = 22$ dBm according to: (a) Load resistance with $C_4 = 3$ nF and $C_5 = 2$ nF and (b) load capacitance with $C_4 = 3$ nF and $R_{load} = 0.43$ k Ω .

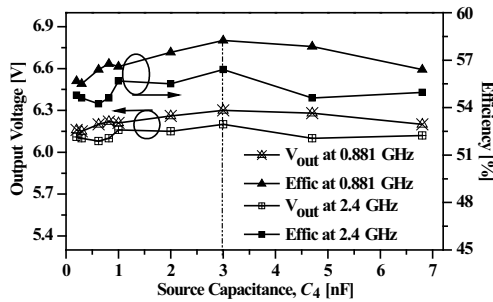


Figure 3. Measured RF-DC conversion efficiency and output voltage of RF-DC converter according to source capacitance (C_4) with $P_{in} = 22$ dBm, $R_{load} = 0.43$ k Ω , and $C_5 = 2$ nF.

the capacitance (C_5) with the fixed C_4 , R_{load} , and P_{in} . In this figure, the output voltage and efficiency are almost constant for all values of C_5 . Among these values, $C_5 = 2$ nF has been chosen. Fig. 3 shows the measured output voltage and RF-DC conversion efficiency according to the source capacitance (C_4) with the fixed C_5 , R_{load} , and P_{in} . The output voltage and conversion efficiency are almost constant in the range of C_4 over 2–6 nF. However, $C_4 = 3$ nF provides the highest output voltage and high efficiency. From these measurement results, the optimized values of R_{load} , C_4 , and C_5 for the high conversion efficiency are given as 0.43 k Ω , 3 nF, and 2 nF, respectively.

2.2. Frequency Selective Dual-band Impedance M/N

The impedance transformers or M/Ns are basic design issues in the RF circuits and systems. The primary function of impedance matching is to reduce the reflection between two connected circuits and to allow the maximum power transfer to the load [16]. The M/N designer mainly pays attention to the impedance match between two consecutive circuits at the operating frequency and rarely considers the out-of-band suppression characteristics. If the M/N can match the operating signal band and suppress the out-of-band unwanted signals simultaneously, then it can also ease the filtering burden of the RF front-end.

Two steps are required to realize the proposed dual-band M/N. In first step, a T-type single band M/N is designed at each operating frequency as shown in Figs. 4(a) and 4(b). Each arm of the T-type single band M/N can be realized with the inductors or capacitors. Although a simple L-type M/N can be used, the T-type M/N is adopted for the out-of-band attenuation characteristics. The π -

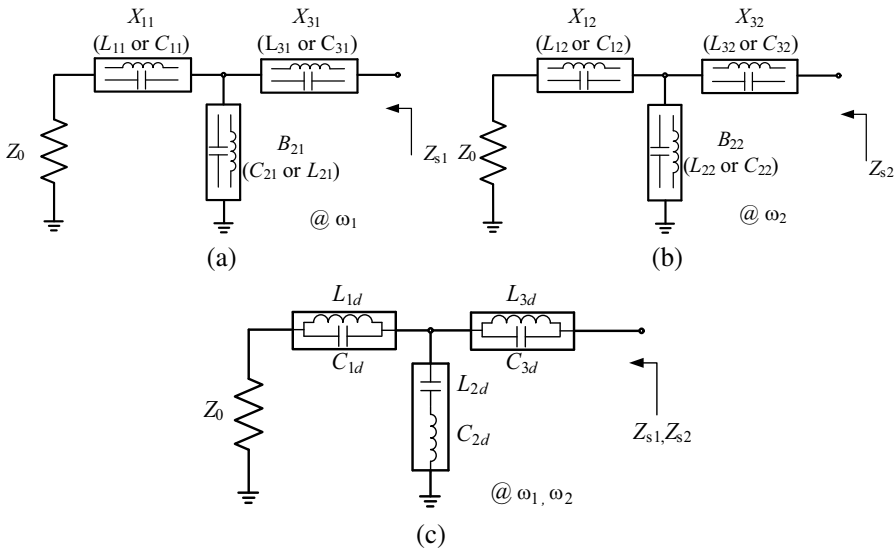


Figure 4. Composition of dual-band M/Ns: (a) Single band M/N at first band (ω_1), (b) single band M/N at second band (ω_2), and (c) dual-band M/N (ω_1, ω_2).

type M/N can also be used instead of the T-type because of their duality characteristics. In second step, two single band M/Ns can be converted into the dual-band M/N by the compliance of reactance and susceptance at the single band M/N.

Figure 4(c) shows the proposed structure of the dual-band M/N which consists of three LC resonators. The series arms of the T-type M/N are realized with the parallel LC, namely series-parallel LC, whereas the shunt arm of the T-type M/N is realized with the series LC, namely shunt-series LC. In Fig. 4, the subscripts i and j in the form of X_{ij} , B_{ij} , L_{ij} , and C_{ij} represent the circuit element number and operating frequency number, respectively. Also, i and d in L_{id} and C_{id} represent the circuit element number and dual-band, respectively. The proposed dual-band M/N can simultaneously match two operating frequency band impedances and provide three transmission zeros at the out-of-band frequencies.

The lumped element values of the dual-band M/N are derived from the reactances and susceptances of two single band T-type M/Ns. As shown in Fig. 5(a), the input impedance of series-parallel LC is equal to the reactance X_{mk} ($m = 1$ or 3) which is given as follows.

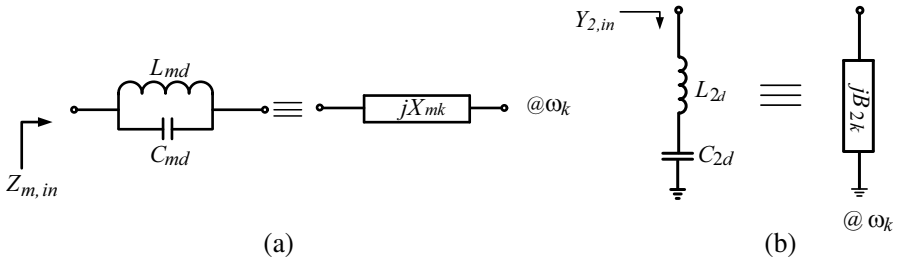


Figure 5. Characteristics of LC resonators: (a) Series-parallel resonators ($m = 1$ or 3) and (b) shunt-series resonator.

$$Z_{m,in} = \frac{j\omega_k L_{md}}{1 - \omega_k^2 L_{md} C_{md}} = jX_{mk} \quad (3)$$

where m and k are the circuit element number and operating frequency band, respectively.

Setting two frequency bands as $k = 1$ and $k = 2$ in (3), the capacitances and inductances of series-parallel resonators are given by (4) and (5).

$$C_{md} = \frac{X_{m2}\omega_1 - X_{m1}\omega_2}{X_{m1}X_{m2}(\omega_2^2 - \omega_1^2)} \quad (4)$$

$$L_{md} = \frac{X_{m1}X_{m2}(\omega_2^2 - \omega_1^2)}{\omega_1\omega_2(X_{m2}\omega_2 - X_{m1}\omega_1)} \quad (5)$$

where X_{m1} and X_{m2} are the reactance of the first band (ω_1) and second band (ω_2), respectively. Similarly, the input admittance of shunt-series LC in Fig. 5(b) is equal to the susceptance B_{2k} which is expressed as follows.

$$Y_{2,in} = \frac{j\omega_k C_{2d}}{1 - \omega_k^2 L_{2d} C_{2d}} = jB_{2k} \quad (6)$$

By applying $k = 1$ and 2 in (6), the element values of the shunt-series resonator shown in Fig. 4(c) are given as follows.

$$L_{2d} = \frac{\omega_1 B_{22} - \omega_2 B_{21}}{B_{21} B_{22} (\omega_2^2 - \omega_1^2)} \quad (7)$$

$$C_{2d} = \frac{B_{21} B_{22} (\omega_2^2 - \omega_1^2)}{\omega_1 \omega_2 (\omega_2 B_{22} - \omega_1 B_{21})}, \quad (8)$$

where B_{21} and B_{22} are the susceptance of the first and second-band M/N, respectively.

Table 1. Condition of series-parallel LC .

$C_{md} = \frac{X_{m2}\omega_1 - X_{m1}\omega_2}{X_{m1}X_{m2}(\omega_2^2 - \omega_1^2)}, \quad (4) \quad L_{md} = \frac{X_{m1}X_{m2}(\omega_2^2 - \omega_1^2)}{\omega_1\omega_2(X_{m2}\omega_2 - X_{m1}\omega_1)}, \quad m=1, 3 \quad (5)$	
<p>1) $X_{m1} > 0, X_{m2} > 0$:</p> $X_{m2}\omega_2 - X_{m1}\omega_1 > 0 \rightarrow X_{m2} > \frac{\omega_1}{\omega_2} X_{m1}$ $X_{m2}\omega_1 - X_{m1}\omega_2 > 0 \rightarrow X_{m2} > \frac{\omega_2}{\omega_1} X_{m1}$	
$\therefore X_{m2} > \frac{\omega_2}{\omega_1} X_{m1}, \quad \frac{\omega_2 L_{m2}}{\omega_2} > \frac{\omega_1 L_{m1}}{\omega_1}$	$L_{m1} < L_{m2}$
$\therefore 0 < X_{m1} < X_{m2}$	$L_{m1}, L_{m2} \text{ are inductance of series arm of single band M/N}$
<p>2) $X_{m1} < 0, X_{m2} < 0$:</p> $X_{m2}\omega_2 - X_{m1}\omega_1 > 0 \rightarrow X_{m2} > \frac{\omega_1}{\omega_2} X_{m1}$ $X_{m2}\omega_1 - X_{m1}\omega_2 > 0 \rightarrow X_{m2} > \frac{\omega_2}{\omega_1} X_{m1}$	
$\therefore X_{m2} > \frac{\omega_1}{\omega_2} X_{m1}, \quad \frac{-\omega_2}{\omega_2 C_{m2}} > \frac{-\omega_1}{\omega_1 C_{m1}}$	$C_{m1} < C_{m2}$
$\therefore X_{m1} < X_{m2} < 0$	$C_{m1}, C_{m2} \text{ are capacitance of series arm of single band M/N}$
<p>3) $X_{m1} > 0, X_{m2} < 0$: $X_{m2}\omega_2 - X_{m1}\omega_1 < 0$ and $X_{m2}\omega_1 - X_{m1}\omega_2 < 0$ always satisfied</p>	
<p>4) $X_{m1} < 0, X_{m2} > 0$: Out-of-condition</p>	

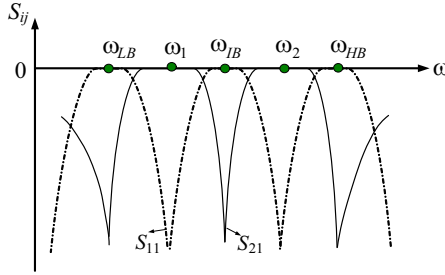
**Figure 6.** Transmission zeros characteristic.

Table 1 and Table 2 show several cases to obtain the positive inductances and capacitances of the series-parallel and shunt-series LC in the dual-band impedance M/Ns. Analysis of the different cases reveals that the inductances and capacitances of the second band M/N must be higher than those of the first band M/N in order to obtain a dual-band M/N assuming that ω_2 is higher than ω_1 . Fig. 6 shows a typical transfer and reflection characteristic (S_{21} and S_{11}) of the proposed frequency limited dual-band impedance M/N with two

Table 2. Condition of shunt-series LC .

$L_{2d} = \frac{\omega_1 B_{22} - \omega_2 B_{21}}{B_{21} B_{22} (\omega_2^2 - \omega_1^2)} \quad (7)$	$C_{2d} = \frac{B_{21} B_{22} (\omega_2^2 - \omega_1^2)}{\omega_1 \omega_2 (\omega_2 B_{22} - \omega_1 B_{21})} \quad (8)$
<p>1) $B_{21} > 0, B_{22} > 0$:</p> $\left. \begin{aligned} \omega_1 B_{22} - \omega_2 B_{21} > 0 &\rightarrow B_{22} > \frac{\omega_2}{\omega_1} B_{21} \\ \omega_2 B_{22} - \omega_1 B_{21} > 0 &\rightarrow B_{22} > \frac{\omega_1}{\omega_2} B_{21} \end{aligned} \right] \begin{aligned} \therefore B_{22} > \frac{\omega_2}{\omega_1} B_{21}, \quad \frac{\omega_2 C_{22}}{\omega_2} > \frac{\omega_1 C_{21}}{\omega_1} \\ C_{21} < C_{22} \\ \therefore 0 < B_{21} < B_{22} \end{aligned}$ <p style="text-align: right;">C_{21}, C_{22} are capacitance of shunt circuit of single band M/N</p>	
<p>2) $B_{21} < 0, B_{22} < 0$:</p> $\left. \begin{aligned} \omega_1 B_{22} - \omega_2 B_{21} > 0 &\rightarrow B_{22} > \frac{\omega_2}{\omega_1} B_{21} \\ \omega_2 B_{22} - \omega_1 B_{21} > 0 &\rightarrow B_{22} > \frac{\omega_1}{\omega_2} B_{21} \end{aligned} \right] \begin{aligned} \therefore B_{22} > \frac{\omega_1}{\omega_2} B_{21}, \quad \frac{\omega_2}{\omega_2 L_{22}} > \frac{\omega_1}{\omega_1 L_{21}} \\ L_{21} < L_{22} \\ \therefore B_{21} < B_{22} < 0 \end{aligned}$ <p style="text-align: right;">L_{21}, L_{22} are inductance of shunt circuit of single band M/N</p>	
<p>3) $B_{21} > 0, B_{22} < 0$:</p> <p style="text-align: center;">$\omega_1 B_{22} - \omega_2 B_{21} < 0$ and $\omega_2 B_{22} - \omega_1 B_{21} < 0$ always satisfied</p>	
<p>4) $B_{21} < 0, B_{22} > 0$: Out-of-condition</p>	

operating bands ω_1 and ω_2 . The transmission zero frequencies selected by the designer can be located at the low band (ω_{LB}), intermediate band (ω_{IB}), and high band (ω_{HB}) for the good dual-band operation. In order to realize the selective characteristics, each arm of the T-type dual-band M/N must resonate at one angular frequency among ω_{LB} , ω_{IB} , and ω_{HB} .

The characteristics of the selective dual-band M/N can be determined by finding the input impedance or admittance at each resonator. Analyzing the series-parallel resonators shown in Fig. 5(a), the input impedances are given as (9).

$$Z_{m,in} = \frac{1}{j\omega_i C_{md} \left(\frac{\omega_k}{\omega_i} - \frac{\omega_i}{\omega_k} \right)} \quad (9)$$

where $\omega_i = 1/(L_{md} C_{md})^{0.5}$ and ω_k are the resonant frequency of M/N arms and the operating frequency, respectively, and i can be selected one among LB , IB , and HB . Similarly, the input admittance of the shunt-series resonator can be calculated by (10).

$$Y_{2,in} = \frac{1}{j\omega_i L_{2d} \left(\frac{\omega_k}{\omega_i} - \frac{\omega_i}{\omega_k} \right)} \quad (10)$$

Table 3. Analysis of LC resonator.

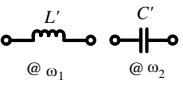
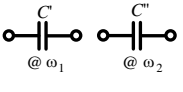
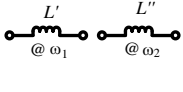
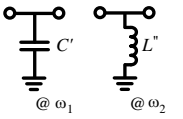
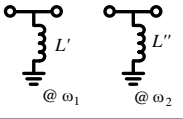
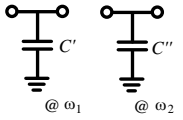
	Conditions	Input impedance	Resonance combination
Series-parallel resonator	Case 1: $\omega_i = 2\pi f_{IB} = \omega_{IB}$	$Z_{m.in} \left \begin{array}{l} \omega_k = \omega_1 \\ \omega_k > \omega_{IB} \end{array} \right. = \frac{1}{j\omega_{IB}C_{md} \left(\frac{\omega_1}{\omega_{IB}} - \frac{\omega_{IB}}{\omega_1} \right)} = \frac{1}{-j\omega_{IB}C'} = j\omega_{IB}L'$	
		$Z_{m.in} \left \begin{array}{l} \omega_k = \omega_2 \\ \omega_k > \omega_{IB} \end{array} \right. = \frac{1}{j\omega_{IB}C_{md} \left(\frac{\omega_2}{\omega_{IB}} - \frac{\omega_{IB}}{\omega_2} \right)} = \frac{1}{j\omega_{IB}C''}$	
	Case 2: $\omega_i = 2\pi f_{LB} = \omega_{LB}$	$Z_{m.in} \left \begin{array}{l} \omega_k = \omega_1 \\ \omega_k > \omega_{LB} \end{array} \right. = \frac{1}{j\omega_{LB}C_{md} \left(\frac{\omega_1}{\omega_{LB}} - \frac{\omega_{LB}}{\omega_1} \right)} = \frac{1}{j\omega_{LB}C'}$	
		$Z_{m.in} \left \begin{array}{l} \omega_k = \omega_2 \\ \omega_k > \omega_{LB} \end{array} \right. = \frac{1}{j\omega_{LB}C_{md} \left(\frac{\omega_2}{\omega_{LB}} - \frac{\omega_{LB}}{\omega_2} \right)} = \frac{1}{j\omega_{LB}C''}$	
	Case 3: $\omega_i = 2\pi f_{HB} = \omega_{HB}$	$Z_{m.in} \left \begin{array}{l} \omega_k = \omega_1 \\ \omega_k < \omega_{HB} \end{array} \right. = \frac{1}{j\omega_{HB}C_{md} \left(\frac{\omega_1}{\omega_{HB}} - \frac{\omega_{HB}}{\omega_1} \right)} = -j\omega_{HB}C' = j\omega_{HB}L'$	
		$Z_{m.in} \left \begin{array}{l} \omega_k = \omega_2 \\ \omega_k < \omega_{HB} \end{array} \right. = \frac{1}{j\omega_{HB}C_{md} \left(\frac{\omega_2}{\omega_{HB}} - \frac{\omega_{HB}}{\omega_2} \right)} = \frac{1}{-j\omega_{HB}C''} = j\omega_{HB}L''$	
Shunt-series resonator	Case 1: $\omega_i = 2\pi f_{IB} = \omega_{IB}$	$Y_{2.in} \left \begin{array}{l} \omega_k = \omega_1 \\ \omega_k < \omega_{IB} \end{array} \right. = \frac{1}{j\omega_{IB}L_{2d} \left(\frac{\omega_1}{\omega_{IB}} - \frac{\omega_{IB}}{\omega_1} \right)} = \frac{1}{-j\omega_{IB}L'} = j\omega_{IB}C'$	
		$Y_{2.in} \left \begin{array}{l} \omega_k = \omega_2 \\ \omega_k > \omega_{IB} \end{array} \right. = \frac{1}{j\omega_{IB}L_{2d} \left(\frac{\omega_2}{\omega_{IB}} - \frac{\omega_{IB}}{\omega_2} \right)} = \frac{1}{j\omega_{IB}L''}$	
	Case 2: $\omega_i = 2\pi f_{LB} = \omega_{LB}$	$Y_{2.in} \left \begin{array}{l} \omega_k = \omega_1 \\ \omega_k > \omega_{LB} \end{array} \right. = \frac{1}{j\omega_{LB}L_{2d} \left(\frac{\omega_1}{\omega_{LB}} - \frac{\omega_{LB}}{\omega_1} \right)} = \frac{1}{j\omega_{LB}L'}$	
		$Y_{2.in} \left \begin{array}{l} \omega_k = \omega_2 \\ \omega_k > \omega_{LB} \end{array} \right. = \frac{1}{j\omega_{LB}L_{2d} \left(\frac{\omega_2}{\omega_{LB}} - \frac{\omega_{LB}}{\omega_2} \right)} = \frac{1}{j\omega_{LB}L''}$	
	Case 3: $\omega_i = 2\pi f_{HB} = \omega_{HB}$	$Y_{2.in} \left \begin{array}{l} \omega_k = \omega_1 \\ \omega_k < \omega_{HB} \end{array} \right. = \frac{1}{j\omega_{HB}L_{2d} \left(\frac{\omega_1}{\omega_{HB}} - \frac{\omega_{HB}}{\omega_1} \right)} = \frac{1}{-j\omega_{HB}L'} = j\omega_{HB}C'$	
		$Y_{2.in} \left \begin{array}{l} \omega_k = \omega_2 \\ \omega_k < \omega_{HB} \end{array} \right. = \frac{1}{j\omega_{HB}L_{2d} \left(\frac{\omega_2}{\omega_{HB}} - \frac{\omega_{HB}}{\omega_2} \right)} = \frac{1}{-j\omega_{HB}L''} = j\omega_{HB}C''$	

Table 3 shows different resonant conditions of the series-parallel and shunt-series LC networks at each frequency. As shown in Table 3, the input impedance or admittance can be equivalent to the inductor or capacitor, depending on the sign of the denominator of (9) and (10).

Even though three transmission zeros are located separately, the transmission zeros can be duplicated at specific band among ω_{LB} , ω_{IB} , and ω_{HB} according to the application. This choice gives freedom to the designers for selecting the M/N topology. To validate the proposed selective dual-band M/N, the two source impedances, $Z_{S_1} = 52.186 + j27.686 \Omega$ and $Z_{S_2} = 57.037 + j16.205 \Omega$, are extracted from

the diode in the high efficient dual-band RF-DC converter at the two operating center frequencies of 881 MHz and 2.4 GHz, respectively, with P_{in} 22 dBm, using a source-pull method. As mentioned earlier in Section 2.2, the two T-type M/Ns operating at individual bands are first designed to match both impedances to the $50\ \Omega$ of the antenna impedance.

The Smith chart tool of ADS 2011 is used to design T-type single band M/N of the both bands. Fig. 7(a) shows the single band T-type M/N with the circuit element values $L_{11} = 4.82\ \text{nH}$, $C_{21} = 2.85\ \text{pF}$, and $L_{31} = 9.54\ \text{nH}$ at the first band (881 MHz). Similarly, Fig. 7(b) shows the T-type M/N at the second band with the circuit element values $C_{12} = 1.33\ \text{pF}$, $L_{22} = 3.55\ \text{nH}$, and $C_{32} = 2\ \text{pF}$.

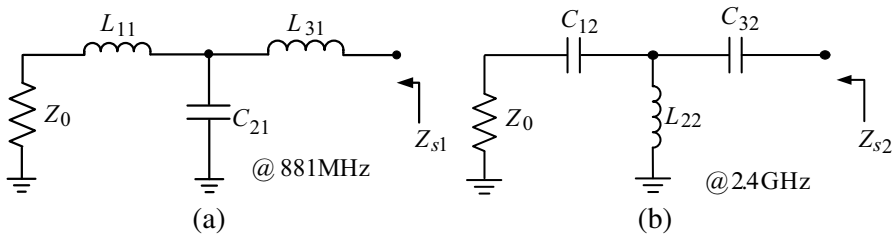


Figure 7. T-type single band M/N: (a) At the first band (881 MHz) and (b) at the second band (2.4 GHz).

Using the reactances and susceptances of the two single band M/Ns, the proposed dual-band M/N was realized. The capacitances and inductances of the series-parallel LC can be calculated from (4) and (5), respectively. The inductance and capacitance of the shunt-series LC can be calculated from (7) and (8), respectively. From the calculation, the component values of the proposed dual-band M/N shown in Fig. 4(c) are $L_{1d} = 3.48\ \text{nH}$, $C_{1d} = 2.591\ \text{pF}$, $L_{2d} = 5.89\ \text{nH}$, $C_{2d} = 1.88\ \text{pF}$, $L_{3d} = 5.203\ \text{nH}$, and $C_{3d} = 2.84\ \text{pF}$. Also, using (9) and (10), the transmission zeros frequencies are calculated as 1.309, 1.51, and 1.676 GHz, which are between the passbands, providing good isolation.

The lumped elements such as inductors are generally available only for a limited range of values and have low-quality factors (Q). Therefore, a high impedance transmission line can be used in this work instead of the lumped inductor. Fig. 8 shows a transmission line and its lumped element equivalent circuit. The electrical length (θ) and characteristic impedance (Z_t) of the transmission line can be derived by comparing the $ABCD$ parameter of the transmission line and its equivalent lumped element circuit [20] as shown in Fig. 8 and given as

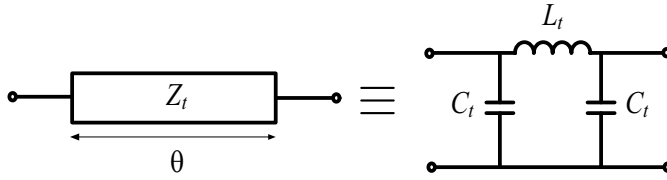


Figure 8. Transmission line and its equivalent lumped element circuit.

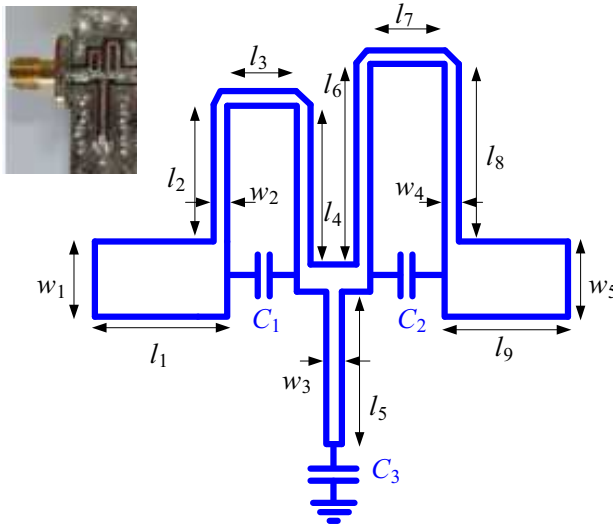


Figure 9. Layout of dual-band matching circuit and physical dimensions: $w_1 = w_5 = 2.4$, $l_1 = l_9 = 3.5$, $l_2 = 3$, $l_3 = l_7 = 1$, $l_4 = 3.7$, $w_2 = 0.37$, $l_5 = 10.8$, $w_3 = 0.6$, $l_6 = 5.25$, $l_8 = 4.55$, $w_4 = 0.51$, $C_1 = 3.2$ pF, $C_2 = 1.8$ pF, $C_3 = 4$ pF. (Physical unit: mm).

(11) and (12).

$$L_t = \frac{Z_t \sin \theta}{\omega} \quad (11)$$

$$C_t = \frac{1 - \cos \theta}{Z_t \omega \sin \theta} \quad (12)$$

As seen from these equations, the high impedance transmission line can approximate as the series inductor. Fig. 9 shows the layout and physical dimensions of the distributed dual-band M/Ns. The circuit was fabricated on a Rogers RT/duroid 5880 substrate with a dielectric constant (ϵ_r) of 2.2 and a thickness (h) of 31 mils.

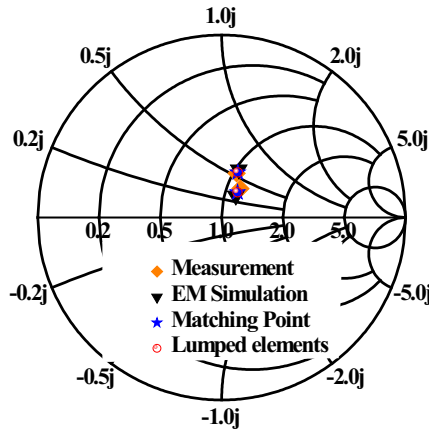


Figure 10. Simulation and measurement result of dual-band matching impedance.

Figure 10 shows the simulation and measurement results of input source impedances of the dual-band M/N and the values are summarized in Table 4. As seen in the table, the measured results have good agreement with the extracted single-band matching impedances.

Table 4. Summary of source impedances at $P_{in} = 22$ dBm.

Items	$Z_{s1}@ 0.881$ GHz	$Z_{s2}@ 2.4$ GHz
Extracted impedance	$52.186 + j 27.686$	$57.037 + j 16.205$
Dual-Band lumped matching circuit simulation	$52.26 + j 27.584$	$57.049 + j 16.212$
Dual-Band matching circuit EM simulation	$51.93 + j 28.255$	$56.51 + j 13.84$
Measurement	$51.746 + j 26.813$	$58.123 + j 18.934$

2.3. Wideband Low-Pass Filter

The RF-DC converter usually needs an output LPF in order to suppress all harmonics made by the diodes as mentioned in [5, 6, 8–13, 21, 22]. In the case of the dual-band RF-DC converter, the generated harmonics are more complicated than those of the single

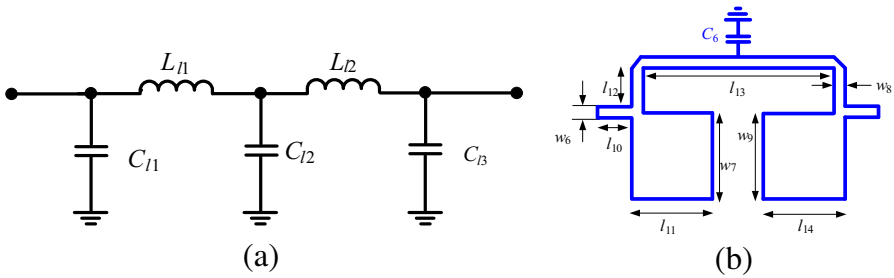


Figure 11. Designed LPF and layout: (a) Conventional lumped element LPF and (b) proposed semi-lumped LPF layout ($C_6 = 15$ pF, $w_6 = w_8 = 0.32$, $l_{10} = 2$, $l_{11} = l_{14} = 5$, $w_7 = w_9 = 5.5$, $l_{12} = 2$, $l_{13} = 12.2$, physical unit: mm).

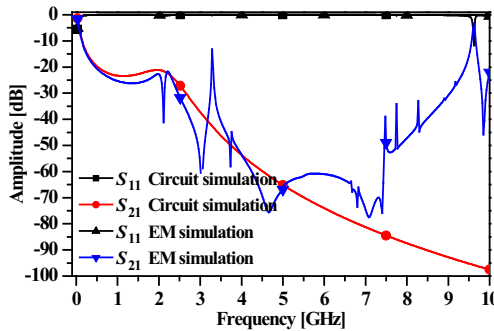


Figure 12. S -parameter of semi-lumped elements LPF and conventional LPF.

band. Therefore, a wideband LPF is required for the high efficient dual-band RF-DC converter. Even though the conventional lumped element LPF, shown in Fig. 11 (a), can be realized with small size, the exact element values cannot be obtained easily with the commercial products. Therefore, instead of lumped elements, the high and low-impedance transmission lines can be used as the series inductor and the shunt capacitors. Therefore, the proposed wideband semi-lumped LPF is depicted in Fig. 11(b) with the physical dimension. The shunt capacitor C_6 is the same as that of C_{l2} and helps to tune the desired cutoff frequency.

Figure 12 shows a comparison between the EM simulation result of the semi-lumped elements LPF and the conventional LPF. The termination impedances of this LPF are 0.43 k Ω in order to match the load resistance (R_{load}). From the EM simulation result, the cutoff

frequency is at 50 MHz and has a better attenuation than 15 dB (from 280 MHz to 9 GHz). The element values for the conventional LPF are $C_{l1} = C_{l3} = 0.3$ pF, $L_{l1} = L_{l2} = 17$ nH, and $C_{l2} = 15$ pF. The difference between the simulated performance of the conventional and the proposed semi-lumped element LPF are due to the frequency dependent characteristics of the transmission lines [23]. Since the amplitudes of the harmonics of the dual-band RF-DC conversion circuit are small at over 7.5 GHz, the EM simulation performance of the semi-lumped LPF can be applicable to suppress these harmonics.

3. MEASUREMENT RESULTS

For the experimental validation, the dual-band RF-DC converter was designed and fabricated. Fig. 13 shows the measurement results of the output voltage and the RF-DC conversion efficiency according to P_{in} . The output voltages and efficiency are first measured at the individual single input power. In this case, the output voltage almost linearly increases as the P_{in} increases. The conversion efficiency also increases as the P_{in} increases from 1 mW to 40 mW and starts to saturate when the P_{in} exceeds 40 mW. When the input power is 158.49 mW (22 dBm), the maximum output voltage of 7.09 V and conversion efficiency of 73.76% are obtained at 881 MHz, whereas 6.86 V and 69.05% are obtained at 2.4 GHz.

When two input signals with the overall power of 158.49 mW (22 dBm) are fed simultaneously, the maximum output voltage of 7.25 V and conversion efficiency of 77.13% are obtained. The detecting output voltage and conversion efficiency of the dual-band signals are slightly higher than those of the single band input signal with the same power level. Because dual-band signals can pass through a dual-band M/N to the diode, the diode can experience higher peak voltage than the single signal.

Figure 14 shows the measurement result of the dual-band RF-DC converter without output LPF. When the individual single signal with the P_{in} of 158.49 mW is fed to the RF-DC converter, the maximum output voltage of 6.49 V and conversion efficiency of 61.8% are obtained at 881 MHz, whereas 6.25 V and 57.14% are obtained at 2.4 GHz. Moreover, the output voltage of 6.76 V and conversion efficiency of 67.05% are obtained in case two input signals with overall signal power of 158.49 mW are fed simultaneously. These maximum output voltages and conversion efficiencies are lower than those of the RF-DC converter with the LPF. As described in [9], these results show the necessity of harmonics suppression. Thus, it is proved that the output voltage and efficiency can be enhanced by suppressing harmonics with the

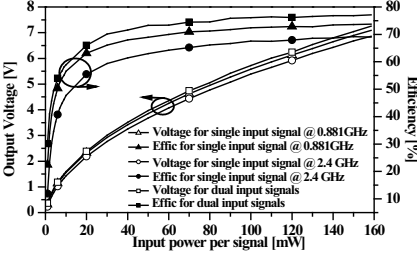


Figure 13. Measurement results of output voltage and RF-DC conversion efficiency using LPF.

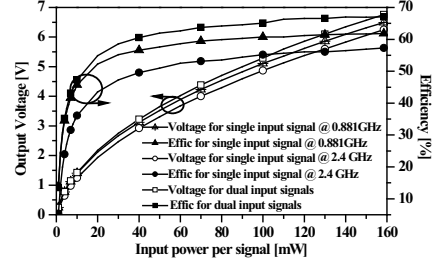


Figure 14. Measurement results of voltage and efficiencies without LPF.

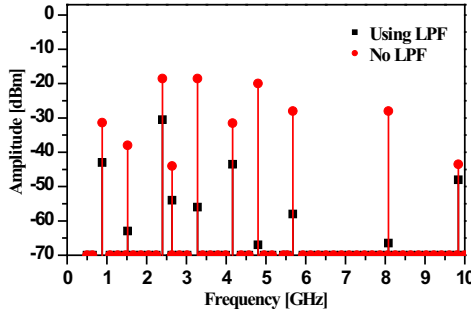


Figure 15. Measured harmonic components of dual-band RF-DC conversion with and without wideband low-pass filter ($@P_{in} = 22$ dBm/tone).

wideband LPF.

Figure 15 shows the measurement results of the harmonic components of the dual-band RF-DC converter with and without the LPF. From this measurement, it is seen that the harmonics generated by nonlinear diodes are suppressed with the proposed wideband LPF.

Figure 16 shows the measured reflection coefficient of the dual-band RF-DC converter and the photograph of the fabricated circuit board. The input signal with 10 dBm is fed to the circuit and the input return losses (S_{11}) are obtained as 17.756 dB and 22.861 dB at the first band and the second band, respectively. From this measurement and Fig. 6, it is evident that the proposed dual-band M/N can match the diode impedances at two operating frequencies and can provide good out-of-band suppression characteristics. The overall size of the fabricated board is 33×25 mm².

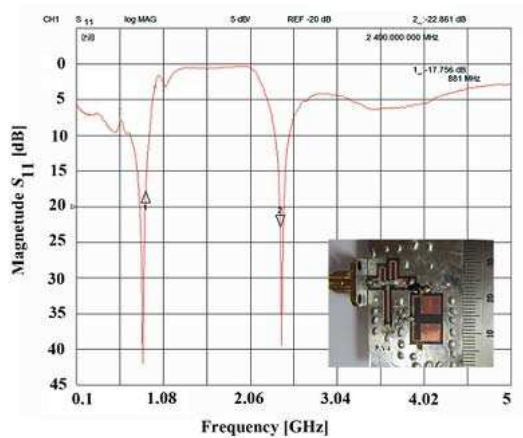


Figure 16. Measured S -parameter of dual-band RF-DC conversion circuit at $P_{in} = 10$ dBm.

4. CONCLUSION

In this work, a highly efficient RF-DC conversion circuit using a novel dual-band M/N and wideband LPF is proposed. The dual-band M/N is analyzed, fabricated, and measured with two operating frequencies 881 MHz and 2.4 GHz. The proposed dual-band M/N can match two receiving band signals simultaneously and effectively suppress the out-of-band signals. A small signal test has been performed to validate the out-of-band suppression as well as in-bands matching characteristics. The proposed wideband low-pass filter can enhance the conversion efficiency and output voltage by suppressing the harmonics generated by the nonlinear diode over the wide frequencies. The proposed dual-band RF-DC conversion circuit can use the two radiated RF signal sources simultaneously and obtain high output voltage and efficiency with the relatively weak signals when compared with the single band strong signal. We are convinced that the proposed dual-band M/N can be applicable with the RF-DC conversion circuit and other microwave multi-band/mode circuit designs.

ACKNOWLEDGMENT

This work was supported by Ministry of Trade, Industry & Energy (MOTIE) and IDEC Platform center (IPC).

REFERENCES

1. Marincic, A. S., "Nikola tesla and the wireless transmission of energy," *IEEE Trans. Power Apparatus and Systems*, Vol. 101, No. 10, 4064–4068, Oct. 1982.
2. Ali, M., G. Yang, and R. Dougal, "A new circularly polarized rectenna for wireless power transmission and data communication," *IEEE Antennas and Wireless Propagation Letters*, Vol. 4, 205–208, 2005.
3. Monti, G., F. Congedo, D. De Donno, and L. Tarricone, "Monopole-based rectenna for microwave energy harvesting of UHF RFID systems," *Progress In Electromagnetics Research C*, Vol. 31, 109–121, 2012.
4. Huang, W., B. Zhang, X. Chen, K. Huang, and C. Liu, "Study on an S-band rectenna arrays for wireless microwave power transmission," *Progress In Electromagnetics Research*, Vol. 135, 747–758, 2013.
5. Park, J. Y., S. M. Han, and T. Itoh, "A rectenna design with harmonic-rejecting circular-sector antenna," *IEEE Antennas and Wireless Propagation Letters*, Vol. 3, 52–54, 2004.
6. Ren, Y. J. and K. Chang, "New 5.8-GHz circularly polarized retrodirective rectenna arrays for wireless power transmission," *IEEE Trans. Microwave Theory Tech.*, Vol. 54, No. 7, 2970–2976, Jul. 2006.
7. Olgum, U., C. C. Chen, and J. L. Volakis, "Investigation of rectenna array configurations for enhanced RF power harvesting," *IEEE Antennas and Wireless Propagation Letters*, Vol. 10, 262–265, 2011.
8. Shinohara, N. and H. Matsumoto, "Experimental study of large rectenna array for microwave energy transmission," *IEEE Trans. Microwave Theory Tech.*, Vol. 46, No. 3, 261–268, Mar. 1998.
9. Chaudhary, G., P. Kim, Y. Jeong, and J. H. Yoon, "Design of high efficiency RF-DC conversion circuit using novel termination networks for RF energy harvesting system," *Microwave Opt. Techno. Lett.*, Vol. 54, No. 10, 2330–2335, Oct. 2012.
10. Gao, Y. Y., X. X. Yang, C. Jiang, and J. Y. Zhou, "A circularly polarized rectenna with low profile for wireless power transmission," *Progress In Electromagnetics Research Letters*, Vol. 13, 41–49, 2010.
11. Shao, X., B. Li, N. Shahshahan, N. Goldsman, T. S. Salter, and G. M. Metzger, "A planar dual-band antenna design for RF energy harvesting applications," *International Semicon. Device Research*

- Symposium*, 1–2, 2011.
12. Li, B., X. Shao, N. Shahshahn, N. Goldsman, T. S. Salter, and G. M. Metzger, “Antenna-coupled dual band RF energy harvester design,” *International Semicon. Device Research Symposium (Student Paper)*, 1–2, 2011.
 13. Heikkinen, J. and M. Kivikoski, “A novel dual-frequency circularly polarized rectenna,” *IEEE Antennas and Wireless Propagation Letters*, Vol. 2, 330–333, 2003.
 14. Suh, Y. H. and K. Chang, “A high-efficiency dual-frequency rectenna for 2.45- and 5.8-GHz wireless power transmission,” *IEEE Trans. Microwave Theory Tech.*, Vol. 50, No. 7, 1784–1789, Jul. 2002.
 15. Ren, Y. J., M. F. Farooqui, and K. Chang, “A compact dual-frequency rectifying antenna with high-orders harmonic-rejection,” *IEEE Trans. Anten. Propag.*, Vol. 55, No. 7, 2110–2113, Jul. 2007.
 16. Pavone, D., A. Buonanno, M. D’Urso, and F. Corte, “Design considerations for radio frequency energy harvesting devices,” *Progress In Electromagnetics Research B*, Vol. 31, 19–35, 2012.
 17. Chang, S. H., W. J. Liao, K. W. Peng, and C. Y. Hsieh, “A Franklin array antenna for wireless charging applications,” *PIERS Online*, Vol. 6, No. 4, 340–344, 2010.
 18. Zhang, J. W., X. Y. Zhang, Z. L. Chen, K. Y. See, C. M. Tan, and S. S. Chen, “On-chip RF energy harvesting circuit for image sensor,” *IEEE 13th Int. Sympo. Integ. Circuit*, 420–423, 2011.
 19. Lin, P. M. and L. O. Chua, “Topological generation and analysis of voltage multiplier circuits,” *IEEE Trans. Circuits and Systems*, Vol. 24, No. 10, 517–530, Oct. 1977.
 20. Park, S., H. Choi, and Y. Jeong, “Microwave group delay time adjuster using parallel resonator,” *IEEE Microwave and Wireless Components Letters*, Vol. 17, No. 2, 109–111, Feb. 2007.
 21. Mbombolo, S. E. F. and C. W. Park, “An improved detector topology for a rectenna,” *IEEE Microwave Workshop Series Innovative Wireless Power Transmission*, 23–26, 2011.
 22. Riviere, S., F. Alicalapa, A. Douyere, and J. D. Lan Sun Luk, “A compact rectenna device at low power level,” *Progress In Electromagnetics Research C*, Vol. 16, 137–146, 2010.
 23. Pozar, D. M., *Microwave Engineering*, 4th Edition, 415–416, Wiley, New York, 2012.